JOURNAL OF AIRCRAFT
Vol. 45, No. 5, September–October 2008

General Mass Capture Model for Swiftly Opening Parachutes

J. Potvin*
Saint Louis University, St. Louis, Missouri 63103

DOI: 10.2514/1.35552

This paper presents a new parachute inflation model that applies to canopies that open very quickly and expand mostly transversely in basically just one inflation stage. Opening swiftness is defined as a process that takes place within the interval $t_{\text{inf 1}} \sim D/V(0)$, where D is a characteristic parachute size scale and $V(0)$ is the fall speed of the parachute payload at the beginning of inflation. This particular inflation mode motivates the use of total and instantaneous capture of the incoming air mass as the dominant fluid flow pattern from which parachute drag is calculated. Together with the use of fixed inflation distance theory, this so-called general mass capture model allows the complete calculation of the evolution of canopy drag and surface area growth as well as of payload-parachute fall rates. As such, this general mass capture scheme should be applicable to unreefed parafoils or to low-porosity hemispherical canopies that are spread over a larger-than-usual initial unfolded area after extraction from the container bag. A comparison with experimental data shows that the general mass capture model can indeed satisfactorily reproduce the drag evolution of both canopy types without involved parameter tuning or curve-fitting. It is noted, however, that such matches do not occur with all drops of canopies deployed repeatedly over the same conditions, thereby suggesting the sporadic, rather than recurrent, character of total mass capture even during swift inflation. Finally, the paper presents several important predictions based on general mass capture, including the value of the opening shock factor C_k being at 2.0 (parafoils) and 2.8 (hemispherical canopies) when the mass of the captured air is much smaller than that of the payload.

Nomenclature

A_{ext}	=	acceleration corresponding to the external for $F_{\text{ext}}(\equiv F_{\text{ext}}/M_{\text{tot}})$
$C(t)$	=	drag function during postinflation
$C_D(t)$	=	drag function during opening $[\equiv SC_D(t)/S(t)]$
C_{D0}	=	steady-state drag coefficient associated with the nominal surface area S_0
C_{init}	=	drag function at the beginning of postinflation
C_k	=	opening shock factor
C_D^{steady}	=	drag coefficient during steady-state descent
D	=	generic canopy size scale
D_0	=	hemispherical canopy nominal diameter
d_{infl}	=	inflation distance
F_D	=	canopy drag
F_{ext}	=	external force applied to the parachute payload
$F_D^{\max}$	=	maximum canopy drag during opening
L	=	span scale associated with the reference collection area
L_{chord}	=	parafoil chord
L_{span}	=	parafoil span
M_{air}	=	captured air mass
M_{tot}	=	total mass [payload and (uninflated) canopy]
n_h	=	nondimensional inflation distance (hemispherical canopies)
n_{infl}	=	nondimensional inflation time
n_p	=	nondimensional inflation distance (parafoils)
q	=	dynamic pressure $[\equiv (1/2)\rho V(t)^2]$
R_{Fd}	=	ratio of added mass drag to form drag term
R_{hemi}	=	surface area ratio [see Eq. (18)]
R_{para}	=	surface area ratio [see Eq. (16)]
$R_m^{(\text{adj})}$	=	drag coefficient-adjusted mass inverse mass ratio
$R_m^{(h)}$	=	mass ratio for hemispherical parachute applications, as defined by gmc
$R_m^{(p)}$	=	mass ratio for parafoil applications, as defined by general mass capture
r	=	radius scale associated with the reference collection area
r_{proj}	=	forward-projected radius of a hemispherical canopy
$S(t)$	=	reference collection reference area
S_{entr}	=	entrainment surface area
$S_{\text{entr}}^{\text{open}}$	=	entrainment surface area at the very end of inflation
S_{final}	=	prescribed final value of the collection area in a general mass capture simulation
S_{proj}	=	forward-projected surface area
$S_{\text{proj}}^{\text{open}}$	=	forward-projected surface area at the very end of inflation
$S_{\text{proj}}^{\text{steady}}$	=	forward-projected surface area during steady-descent
S_0	=	canopy nominal surface area
$SC_D(t)$	=	drag area function $[\equiv 2F_D(t)/\rho V^2(t)]$
t	=	time
t_{infl}	=	inflation time (also canopy expansion time)
$V(t)$	=	speed of the parachute payload, along trajectory
$V(0)$	=	speed at the beginning of inflation
V_i	=	speed at the beginning of postinflation
V_T	=	speed of the system during steady-state descent
Z	=	travel distance of the system along its trajectory
$\tilde{z}$, $\tilde{t}$, $\tilde{F}_{\text{ext}}$, etc.	=	nondimensional versions of the preceding variables and parameters
Γ_{capt}	=	fraction of captured air mass
Δt	=	time increment
ρ	=	air density at opening altitude

Received 7 November 2007; revision received 12 March 2008; accepted for publication 13 April 2008.

*Professor, Department of Physics. Senior Member AIAA.

I. Introduction

BECAUSE of its inherent complexity, the modeling of parachute inflation has been most successful, in terms of fidelity and predictive power, when formulated not only for specific canopy geometry, overall design, and deployment strategy, but also when involving explicit descriptions of the canopy-filling processes

actually taking place. Following this philosophy, a new so-called general mass capture (GMC) model is proposed, wherein the entire air mass that is set into motion by the opening parachute is hypothesized to instantly comove at the same speed with the payload-canopy complex during the entire inflation sequence. Complete mass capture is, of course, the exception rather than the rule in parachute inflation dynamics. However, it should be a dominant feature for those canopies, hemispherical or winglike, that 1) open very swiftly and 2) expand mostly transversely with respect to the direction of fall. Inflation swiftness means an inflation sequence that takes place within a timescale of $t_{\text{infl}} \sim D/V(0)$, where D is a characteristic parachute size scale and $V(0)$ is the fall speed of the parachute payload system at the very beginning of the process. Such a swift opening duration is about 5 to 10 times smaller than that experienced by typical production canopies [1–4].

All inflating hemispherical canopies featuring low geometric porosity and low fabric permeability (i.e., of low total porosity [2]) should capture, as a matter of design, all the air that is directly facing their opened mouths at any given time. But such mouth-collected air is not all the air that is set into motion by inflation. Complete air mass capture shall occur only when the canopy-opening process helps the deflection and entrainment into the parachute's near wake of the nearby moving air that is not lined up with the mouth. In this regard, swift and transverse inflation should promote this process via the generation of a much lower pressure in the wake, relative to the associated stagnation pressure $1/2\rho V(0)^2$ and also relative to the base pressure seen during the steady-state descent regime. Similarly, complete mass capture in the case of parafoils is achieved when most of the oncoming air remains under the wing's bottom skin, a collection process that should be helped by the wings' anhedral and wing-tip stabilizers,[†] and again by the entrainment of nearby air into the wake. With such a definition, swift- and transversely opening parachutes shall include the following cases used in the field nowadays: 1) unreefed parafoils rigged for near-zero glide during opening, 2) parafoils reefed by aerodynamically ineffective sliders, 3) low-porosity hemispherical parachutes featuring a large unfolded and uninflated area after deployment, and 4) low-porosity hemispherical parachutes opening with the aid of pyrotechnic skirt spreaders.

All unreefed parafoils are natural swift openers, given that their spanwise expansion occurs well before actual cell inflation, from the oncoming air impacting their lower surface and pushing the wing's tips and wing's stabilizers outward. Low-porosity hemispherical parachutes, such as military personnel parachutes, can open swiftly also, as a result of unusual dynamics during extraction of the canopy out of its deployment bag. In this case, the canopy may find itself unfolded over a surface area that is greater than normal after bag strip, thus permitting large air fluxes into the canopy at the beginning of inflation. Note that large initial unfolded fabric spreading, as well as large initial opened mouths, can occur as a matter of design as well: for example, with canopies that are packed in oversized bags and/or are attached to very wide payloads (via two sets of risers) or when outfitted with pyrotechnic skirt spreaders, as currently used on the ejection-seat system of the U.S. Marine Corps Harrier attack jet. Finally, slider-reefed parafoils have been known to open swiftly as well, although rarely, in those cases in which the slider has been rendered aerodynamically ineffective. This occurs when the oncoming air is able to insert itself between the slider's top side and the parafoil's bottom skin, in contrast with the usual scenario in which there is no such insertion. A region of high dynamic pressure thus appears on both sides of the slider (instead of only on its bottom side as usual), in effect, canceling the slider's own drag. Slider drag is crucial for keeping the canopy in a reefed configuration during the early part of inflation, in opposing the aerodynamic forces that try to inflate the canopy's cells and expand the canopy's bottom side [1–3]. With its own drag being cancelled, the slider is no longer able to resist such an expansion and instead begins its quick travel downward, under the action of the suspension line fanning from its four corner grommets. The result is an unrestrained and swift expansion of the canopy.

Note that as a matter of design, transverse expansion is the only shape evolution available to parafoil openings. On the other hand, it is quite unusual for most normally opening hemispherical-type canopies, because they tend to evolve from a cigarlike shape, adopted after deployment, to a lightbulblike shape that expands mostly longitudinally. In this case, transverse expansion occurs only at the very end of inflation: namely, when the bulbous section is large enough to encompass the canopy skirt area.

Swift openings are not desirable outcomes because they are accompanied by canopy drag forces that may be high enough to load the canopy well beyond its structural limits. In fact, swift-opening avoidance is usually the prime motivation for the use of reefing, either in the form of sliders or skirt reefing lines [2,3,5]. Despite its rarity, swift inflation deserves further study, given that it will frequently affect prototypes and even production items afflicted by unusual reefing failures (such as the slider drag cancellation effect previously mentioned). Thus, this new GMC inflation model should give parachute engineers a load-prediction tool for worst-case scenarios without resorting to unreasonably large load estimates.

In what follows, the basic principles of the GMC model are discussed first, followed by a quick comparison of its numerical predictions with experimental data collected on two unreefed parafoils and on a subscale unreefed U.S. Air Force C-9 hemispherical parachute. Other interesting aspects shall be discussed as well, including a prediction of the value of the opening shock factor C_k being at about 2.0 for parafoils and at 2.8 for hemispherical canopies in cases in which the mass of the captured air is much smaller than that of the payload. Another set of C_k predictions shall be discussed as well, in the limit in which the captured mass is of the same order of magnitude as that of the payload. Throughout the paper, the formalism for parafoils and hemispherical canopies will be developed in parallel, to show the fundamental differences as well as the similarities that characterize the inflation of each design.

II. Basic Principles

The GMC model shall be based on the standard approach to drag calculation: that is, by directly computing the rate of momentum transfer from the parachute payload system to the air that it sets into motion [6–16] (see [17] for a review). In general, the complexity of the airflow and canopy fabric motions involved in inflation makes this approach impractical, unless specific assumptions are made concerning the canopy's instant shape and the type of flows going into, out of, and about the canopy. Past investigations have shown that inflation force data and photographic data on evolving canopy shape obtained from both wind-tunnel studies and test drops can be used to guide the choice of the most realistic shape, of the correct computed of air mass, and of the transitory values of the drag coefficient [8–10,14,15]. Although this strategy has yielded good results when applied to high-porosity ribbon-type hemispherical parachutes [8–11,17], it has produced rather mixed results in applications involving low-porosity hemispherical parachutes [13–15,18,19].

The situation should be quite different in the case of swiftly opening canopies, given that the air mass being set into motion is hypothesized as having been captured, for the most part, by the canopy payload complex (Fig. 1). Complete mass capture greatly simplifies the calculation of momentum transfer, given that one needs only to consider the air that is oncoming, contrasting with partial air capture, which necessitates a detailed budget of what has been captured and then rereleased [8–11,13–17]. With total mass capture, detailed knowledge about actual canopy shape thus becomes irrelevant to the calculation.

A. Flow Comparisons

Figure 1 shows the flow patterns occurring during swift inflation, in comparison with those seen during the motion of an already-inflated canopy (accelerating or traveling at constant speed). With the

[†]Stabilizers look like the winglets seen on jetliners, except that they are pointing downward and that they have a much wider chord. Stabilizers insure extra directional stability during the landing flare.

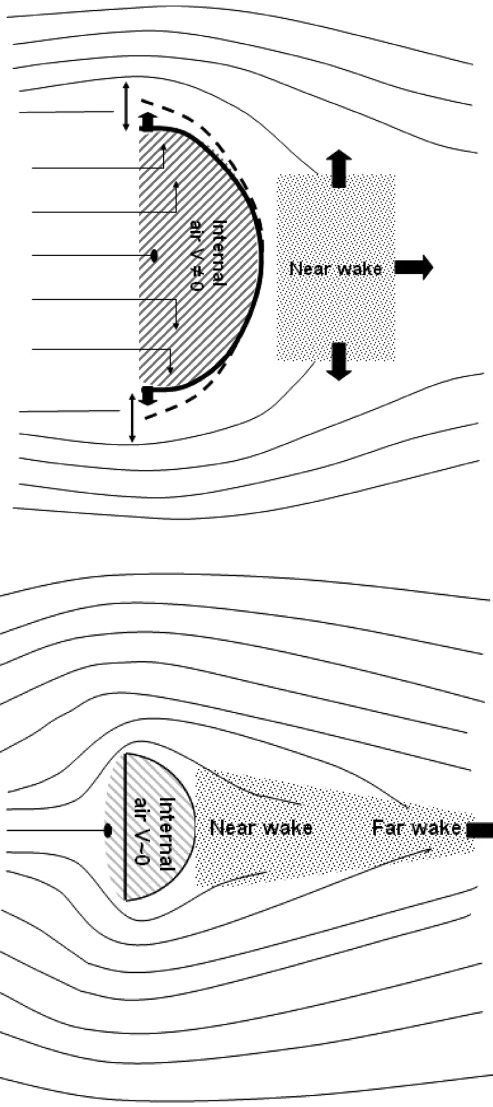

Fig. 1 Schematics of the airflow during swift inflation (top) compared with that of postinflation, steady descent, or accelerating (bottom). The bold solid and dotted lines shown in the top figure correspond to the outline of the opening canopy at times t and $t + \Delta t$.

former, a large portion of the incoming air is permanently being removed from the overall flow that is moving toward and around the canopy, to remain with the canopy-wake system. With an already inflated canopy, a much smaller fraction of the incoming air is being removed, being captured only into both near and far wakes. In this respect, a swiftly inflating canopy acts as a much greater mass sink. Moreover, the flow deflection seen ahead of the already-inflated canopy (and its near absence with an inflating canopy) does suggest that the fraction of streamlines being accelerated past the canopy and wake (namely, the so-called potential flow)[‡] should be much smaller with the latter than with the former.

B. Totally Inelastic Mass Capture Momentum Budget

Seen from a collision perspective, the interaction between the oncoming air and the canopy that captures all of it would be characteristic of a totally inelastic collision. With both parafoil and hemispherical canopy cases, such captured air moves with the parachute payload system at the same speed until the end of the inflation/expansion process (Fig. 2). Note that such an inelastic interaction between airflow and canopy is more the exception than

[‡]Potential flow corresponds to those streamlines that move in an inviscid manner about the canopy *and* wake; as such, this flow can be described by the Euler version of the fluid equations of motion.

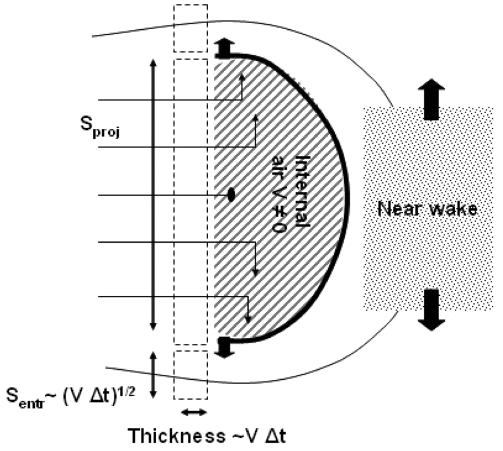

Fig. 2 Outlines of the to-be-captured air parcels during swift openings (dashed lines).

the rule for parachutes inflating in a normal, nonswift, manner. But even for those, this type of collision may be taking place temporarily (i.e., over times that are shorter than the overall inflation timescale) or during specific substages of the inflation process [11,20,21].

The calculation of the momentum lost by the parachute and gained by a captured air parcel proceeds as follows (Fig. 2). The volume of the (oncoming) air to be captured during a small time interval Δt (i.e., between times $t - \Delta t$ and t) is expressed as $S(t)V(t)\Delta t$, with $V(t)$ representing the fall speed of the parachute payload. Here, $V(t)\Delta t$ and $S(t)$ would correspond to the effective thickness and instant reference collection surface area of the parcel, respectively. This reference collection area is further subdivided as $S(t) = S_{\text{proj}}(t) + S_{\text{entr}}(t)$, where, in the case of parafoils, S_{proj} represents the outline of the spread wing and for hemispherical canopies it corresponds to the maximum opened width of the canopy (mouth of the upper surface), projected in the direction of fall. On the other hand, S_{entr} corresponds to the surface area penetrated by the flow captured in the near wake. S_{entr} is represented by rectangular and circular outer rings spanning the instant perimeter of parafoils and hemispherical canopies, respectively (i.e., spanning the area S_{proj}). In both cases, the ring would have a thickness of order $\sim V(t)\Delta t$, as suggested in Fig. 2 (hemispherical canopy). On the other hand, these rings would have widths of order $\sim V(t)\Delta t$ (parafoils) and $\sim (V(t)\Delta t)^2$ (hemispherical canopy), following from the fact that parafoils expand mostly spanwise, whereas hemispherical canopies expand radially. Compared with S_{proj}, the rings' cross-sectional area S_{entr} would therefore be negligible at large enough times: that is, when S_{proj} is itself large (see Figs. 1 and 2). Finally, note that S_{entr} defined here does not incorporate those streamlines associated with potential flow, because it shall be assumed herein that such flow only contributes in a minor way to the overall drag. This can be seen by comparing the momentum gained by the captured air (namely, $\sim \rho \times$ canopy volume $\times (V(t) - 0)$) with that of the potential-flow streamlines that, even when assuming similar mass (there should be less of it), would have $\sim \rho \times$ canopy volume $\times (u(t) - 0)$) [i.e., a much smaller gain, given that $u(t) \ll V(t)$].

Complete mass capture means that at time t, the momentum of the complex composed of the payload, expanding parachute, and air captured so far, is given by

$$\left(M_{\text{tot}} + \int_0^t \mathrm{d}M_{\text{air}}\right) \cdot V(t) \tag{1}$$

where M_{tot} is the combined mass of the payload and (uninflated) parachute. The integral sums up the mass of the captured air, now accumulating, that is inside as well as topside of the canopy: namely,

$$\int_0^t \mathrm{d}M_{\text{air}} = \int_0^t \Gamma_{\text{capt}}\, \mathrm{d}t' \rho S(t') V(t') \tag{2}$$

The right-hand side (RHS) of Eq. (2) follows from the definition of the mass of each incoming parcel that is being set in motion at t: namely, $\Gamma_{\text{capt}}\rho S(t)\Delta t V(t)$. Note the factor Γ_{capt} appearing in Eq. (2), which has been inserted by hand to show the effects of partial mass capture with nonswiftly opening canopies when applicable. For such canopies, the value of Γ_{capt} would be a time-dependent function located within the integral shown in Eq. (2). Moreover, Γ_{capt} should be expected to be somewhat different on a jump-to-jump (or drop-to-drop) basis, given the chaotic nature of the air-shedding process taking place by and inside the near wake. Restricting Eq. (2) to swift inflation demands that $\Gamma_{\text{capt}} \sim 1$, an important simplification.

It should be stressed that in this GMC approach, the value of Δt in Fig. 1 corresponds to the travel time of the canopy payload system. This means that the incoming parcel of mass $\rho S(t)\Delta t V(t)$ must be captured completely during that same timescale. For both parafoil and hemispherical canopies, the air captured on their underside should indeed be trapped within Δt. Whether the entrained air gets captured into the wake during Δt as well remains an open question, although the idea seems intuitively correct.

Returning to momentum transfer computation, the momentum of the parachute payload-trapped-air complex at $t + \Delta t$ changes to

$$\left(M_{\text{tot}} + \int_0^t \mathrm{d}M_{\text{air}}\right) \cdot V(t + \Delta t) + [\rho S(t)\Delta t V(t)] \cdot V(t + \Delta t) \quad (3)$$

Thus, under the influence of an external force F_{ext} such as gravity or propulsion [22], the rate of momentum change over Δt is given by combining Eqs. (1) and (3):

$$\left(M_{\text{tot}} + \int_0^t \mathrm{d}M_{\text{air}}\right) \frac{[V(t + \Delta t) - V(t)]}{\Delta t} + \rho S(t) \cdot V(t)^2 = F_{\text{ext}} \quad (4)$$

Here, $V(t + \Delta t)$ has been replaced by $V(t)$ to result in the V^2 term. Rearranging this result yields the following equation of motion characterizing the parachute payload system represented by M_{tot} (i.e., the system without the captured air):

$$M_{\text{tot}} \frac{\mathrm{d}V}{\mathrm{d}t} = -2S(t) \cdot \left(\frac{1}{2}\rho V(t)^2\right) - \left(\int_0^t \Gamma_{\text{capt}}\, \mathrm{d}t' \rho S(t') V(t')\right) \frac{\mathrm{d}V}{\mathrm{d}t} + F_{\text{ext}} \quad (5)$$

Note that at time $t + \Delta t$, the recently-captured air is now moving at the same speed as that of the parachute and already-captured air; this makes the collision totally inelastic rather than partially inelastic as in most real cases, swiftly inflating or not. The first two terms of the right-hand side represent the net drag force $F_D(t)$ generated by the canopy. In most cases in which the system decelerates during inflation, the value of the derivative $\mathrm{d}V/\mathrm{d}t$ is negative, meaning that the term in $\mathrm{d}V/\mathrm{d}t$ will reduce the contribution of the V^2 term to the canopy's overall drag.

In the following, the instant collection area $S(t) \equiv S_{\text{proj}}(t) + S_{\text{entr}}(t)$ shall be approximated as $S(t) \sim S_{\text{proj}}(t)$, following from S_{entr} being proportional to Δt or to Δt^2. Although quite accurate at large times when $S(t) \gg S_{\text{entr}}(t)$, this approximation shall be quite unrealistic at small times, in cases in which $S(0)$ is small. Interestingly, [14] suggests $S_{\text{entr}}/S_{\text{proj}} \sim 0.18$ at the time of full inflation with low-porosity hemispherical parachutes.

Finally, it should be mentioned again that derivation of Eq. (5) has left out the momentum transfer related to potential-flow acceleration, which has been argued to be small during swift inflation. Moreover, Eq. (5) has also ignored the effects of wing lift, which may occur with parafoils that are good gliders even when partially inflated. In most parafoil applications, lift ability is removed temporarily by rigging to prevent violent canopy surging during inflation. But such removal may be imperfect, as shall be shown in the following comparison with the experiment.

C. Comparison with Explicit Added Mass Formulations

Conceptually, the generality of the derivation of Eq. (5) points to several interesting comparisons: First, the V^2 term corresponds to the rate of momentum transferred to the incoming air slabs. With total capture, the entire air mass contained in the slabs acquires momentum, in contrast to the air of those slabs meeting an already-inflated parachute (moving at constant V), which does not (Fig. 1), hence the higher value of the associated drag coefficient being equal to a value of 2.0 versus 1.0 for inflated parafoils and 1.5 for hemispherical canopies. This reinforces an important point made by Desabrais et al. [19], who demonstrated a similar dichotomy in their wind- and water-tunnel studies of solid (i.e., noninflating) and flexible (i.e., inflating) subscale canopy models. Second, the terms in $M_{\text{air}}\,\mathrm{d}V/\mathrm{d}t$ and $V\,\mathrm{d}M_{\text{air}}/\mathrm{d}t$ usually added to the V^2 term in an ad hoc manner in past explicit added-mass formulations of this problem (see, for example, [7–17]) do not appear explicitly here, instead being implicit in the integral term and V^2 term of Eq. (5), respectively. Both can be derived to appear explicitly, of course, but only once specific canopy shape and expansion rules have been specified. Note, finally, that extra terms in $m\,\mathrm{d}V/\mathrm{d}t$ and $V\,\mathrm{d}m/\mathrm{d}t$ would have appeared in addition to what is currently in the right-hand side of Eq. (5), had the contributions of accelerated potential flow been taken into account. Interestingly, a comparison between the contribution to overall drag by such potential-flow-related terms (i.e., $m\,\mathrm{d}V/\mathrm{d}t$ and $V\,\mathrm{d}m/\mathrm{d}t$) and those derived from the integral term of Eq. (5) (i.e., $M_{\text{air}}\,\mathrm{d}V/\mathrm{d}t$ and $V\,\mathrm{d}M_{\text{air}}/\mathrm{d}t$) has been documented empirically by Desabrais and Johari [18] with canopy models not opening so swiftly.

D. Opening Shock Factor Prediction

An interesting prediction stems from Eq. (5), in cases consisting of very heavy payloads traveling at high speeds, for which $M_{\text{tot}} \gg \rho D^3$ and $D|\mathrm{d}V/\mathrm{d}t| \ll V^2$. Under such conditions, the added mass term can be neglected altogether as $\mathrm{d}V/\mathrm{d}t \sim 0$, thus yielding $F_D(t) = 2S(t)q(t)$, with $q(t) \equiv 1/2\rho V(t)^2$. This in turn means that 1) $F_D(t) \sim 2S(t)q(0)$ and 2) the maximum drag $F_D^{\max}$ is generated at the very end of the inflation process: namely, when the canopy area is equal to the fully opened area (i.e., $S(t) = S_{\text{proj}}^{\text{open}} + S_{\text{entr}}^{\text{open}}$). Under such conditions, one has $F_D^{\max} = 2(S_{\text{proj}}^{\text{open}} + S_{\text{entr}}^{\text{open}})q(0)$. This result becomes quite useful when used to derive the *opening shock factor* C_k, defined as $C_k \equiv F_D^{\max}/(C_{D0}S_0 q(0))$, with C_{D0} corresponding to the steady-state drag coefficient associated with the nominal canopy reference area S_0 [2]. In other words, C_k is a ratio of the drag coefficient sustained at peak loading, over the parachute's steady-state value. The opening shock factor is a useful nondimensionalization of $F_D^{\max}$, because it allows interesting comparisons of the opening characteristics of various parachute designs, after factoring out the explicit dependence on air density, initial speed, and overall canopy size. The GMC model yields a prediction of C_k, here given by

$$C_k = 2\left(1 + S_{\text{entr}}^{\text{open}}/S_{\text{proj}}^{\text{open}}\right)\left(S_{\text{proj}}^{\text{open}}/S_0\right)\Big/ C_{D0}$$

or, after neglecting the entrained area, $C_k = 2(S_{\text{proj}}^{\text{open}}/S_0)/C_{D0}$. In the case of hemispherical canopies, swift inflation ends with the parachute overinflating well beyond its steady-descent projected area $S_{\text{proj}}^{\text{steady}}$ (i.e., $S_{\text{proj}}^{\text{open}} > S_{\text{proj}}^{\text{steady}}$), extending to a value that is nearly equal to the nominal area S_0, but somewhat less than by about 20%. Thus, one has $C_k \sim 2/C_{D0}$, and choosing the lower bound in the known range of drag coefficients for such canopies to partly offset the overestimate for $S_{\text{proj}}^{\text{open}}/S_0$, one arrives at $C_{D0} \sim 2.86$ (using the range $C_{D0} \sim 0.7$–0.8 [2]). Parafoils, on the other hand, have a projected area that is identical to the nominal area and, additionally, do not overinflate by design. Thus, for this case $S_{\text{proj}}^{\text{open}} = S_0$ and $C_k \sim 2$, given that $C_{D0} \sim 1$.

These predicted values are consistent with, but clearly higher than, the world data on C_k for nondecelerating parachute systems [i.e., values residing at about $C_k \sim 1.4$ (on average)]. This difference should be due partly to the world data representing all canopies, including *high-porosity* canopies for which $\Gamma_{\text{capt}} \ll 1$ (and for which the GMC does not apply). It should also be due to the fact that the

world database includes mostly not-so-swiftly-opening canopies and to the fact that the opening shock factor is, in general, inversely proportional to inflation time [4].

E. Coupling Canopy Expansion Rates to Parachute Payload Fall Rates

For all its generality, Eq. (5) cannot be solved until specifics on the evolution of the surface area function $S(t)$ are defined. It is at this stage that another evolution equation describing the transverse motion of selected canopy components must be selected. The GMC model shall rest on a simple supplemental equation: namely, one inspired from fixed inflation distance (FID) theory, in which instant transverse canopy dimensions are set as proportional to the instant travel distance of the canopy payload equation [2].

Fixed inflation distance theory is based on the fact that each parachute design is characterized by a nondimensional inflation time $n_{\text{infl}} = t_{\text{infl}} V(0)/r_{\text{proj}}$, with r_{proj} being the forward-projected diameter of the canopy at full inflation. With heavy payloads attached to small parachutes in which $M_{\text{tot}} \gg \rho r_{\text{proj}}^3$, the system is moving at nearly constant speed, and the existence of n_{infl} implies that the inflation distance d_{infl}, here defined as $d_{\text{infl}} = V(0)t_{\text{infl}}$, is thus given by $d_{\text{infl}} = n_{\text{infl}} r_{\text{proj}}$, thereby yielding the basic FID equation.

The argument leading to FID obviously fails in the case of lighter payloads attached to large canopies, because those are expected to move at decreasing speeds during the inflation process, thus yielding $d_{\text{infl}} = V(0)t_{\text{infl}} + 1/2a(0)t_{\text{infl}}^2 + \mathcal{O}(t_{\text{infl}}^3)$. But for swift inflation in which n_{infl} is basically 5–20 times smaller than the associated normal-inflation durations (being set at $\sim$1), the time allowed for deceleration is much reduced, thus making the FID equation more plausible. Indeed, the empirical data discussed in Sec. IV do show inflation times of order $\sim$0.2 s, in contrast with the same canopies nominally inflating over 2-s intervals. It is clear that in this case, the next-order correction to the basic FID equation [i.e., the term in $1/2a(0)t_{\text{infl}}^2$] would then be reduced by nearly a factor of 100.

In cases in which the transverse motions of the canopy skirt involve speeds that are nearly the same as $V(0)$ (certainly a plausible scenario for swift inflation), FID theory thus implies canopy expansion rates that should be approximately proportional to the parachute payload system's fall rates: namely,

Hemispherical canopy:

$$n_h \sqrt{\pi} \frac{\mathrm{d}r}{\mathrm{d}t} = \frac{\mathrm{d}Z}{\mathrm{d}t} \equiv V(t) \tag{6}$$

Parafoil:

$$n_p \frac{\mathrm{d}L}{\mathrm{d}t} = \frac{\mathrm{d}Z}{\mathrm{d}t} \equiv V(t) \tag{7}$$

Here, the functions r and L represent, respectively, a reference collection radius (for hemispherical canopies) and span (for parafoils), to be related to the collection surface area $S(t)$ and canopy reference area S_{proj} in the next paragraph. On the other hand, the function $Z(t)$ represents the parachute payload displacement along the fall trajectory, either horizontal, vertical, or ballistic.

Parameters n_h and n_p are proportionality constants relating canopy expansion to the fall rates of the parachute payload system. In cases in which the FID concept is not operating, n_h and n_p would then be complicated time functions defined by the specifics of the canopy design (and reefing) and by the actual aerodynamics that control the flow and pressure conditions. For parachutes opening nominally (i.e., not swiftly), n_h and n_p have magnitudes in the range of 5–20. In this paper, both n_h and n_p shall be set to unity, in accordance with the GMC model applying to swift inflation processes in which $t_{\text{inf}\,1} \sim D/V(0)$.

Integrating Eqs. (6) and (7) yields, together with the condition $Z(0) = 0$, the following results:

Hemispherical canopy:

$$n_h \sqrt{\pi}(r(t) - r(0)) = Z(t) \tag{8}$$

Parafoil:

$$n_p(L(t) - L(0)) = Z(t) \tag{9}$$

Equations (8) and (9) can now be used to define the instant collection reference area $S(t)$, given the definitions $S(t) \equiv \pi r(t)^2$ (hemispherical canopies) and $S(t) \equiv L_{\text{chord}} L(t)$ (parafoils). Note that here L_{chord} is the chord length, usually an unchanging parameter:

Hemispherical canopy:

$$S(t) = \frac{Z(t)^2}{n_h^2} + 2\sqrt{S(0)} \frac{Z(t)}{n_h} + S(0) \tag{10}$$

Parafoil:

$$S(t) = \frac{Z(t) L_{\text{chord}}}{n_p} + S(0) \tag{11}$$

Comparing Eqs. (10) and (11) shows one fundamental difference between parafoil and hemispherical parachute inflation: namely, their linear and quadratic dependence on parachute payload travel distance. With expansion laws such as Eqs. (10) and (11), the GMC model now becomes fully defined and ready for a complete solution.

III. Numerical Solutions

A. Final Equations of Motion

Equation (5) can be solved once Eqs. (10) and (11) are used for the computation of its integral; its final form is

Parafoil:

$$\left\{ M_{\text{tot}} + \Gamma_{\text{capt}} \rho \left(\frac{Z(t)^2 L_{\text{chord}}}{2n_p} + S(0) Z(t) \right) \right\} \frac{\mathrm{d}^2 Z}{\mathrm{d}t^2} = \left\{ -2 \left(\frac{Z(t) L_{\text{chord}}}{n_p} + S(0) \right) \cdot \left(\frac{1}{2} \rho \left(\frac{\mathrm{d}Z}{\mathrm{d}t} \right)^2 \right) \right\} \tag{12}$$

Hemispherical canopy:

$$\left\{ M_{\text{tot}} + \Gamma_{\text{capt}} \rho \left(\frac{1}{3n_h^2} Z(t)^3 + \frac{\sqrt{S(0)}}{n_h} Z(t)^2 + S(0) Z(t) \right) \right\} \frac{\mathrm{d}^2 Z}{\mathrm{d}t^2} = \left\{ -2 \left(\frac{Z(t)^2}{n_h^2} + 2\sqrt{S(0)} \frac{Z(t)}{n_h} + S(0) \right) \cdot \left(\frac{1}{2} \rho \left(\frac{\mathrm{d}Z}{\mathrm{d}t} \right)^2 \right) \right\} \tag{13}$$

In deriving both Eqs. (12) and (13), the external force F_{ext} has been set to zero, given that the experimental data used in the upcoming comparison have been collected on canopies that opened mostly along the horizontal.

B. Input Parameters

In what follows, the values of the parameters Γ_{capt}, n_p, and n_h will be set to unity for the reasons mentioned earlier; the philosophy behind the comparison with the experiment is the validation of the ideas behind GMC, not the production of a best fit. Nevertheless, Γ_{capt}, n_p, and n_h will continue to appear symbolically in Eqs. (12) and (13) and elsewhere, to show explicitly where in the formalism the amount of captured mass and the Z–S coupling rates do enter.

The numerical solutions of Eqs. (12) and (13) are evolutions in time, which will be stopped when the collection reference surface area $S(t)$ reaches the value $S_{\text{final}} = S_{\text{proj}}^{\text{open}} + S_{\text{entr}}^{\text{open}}$. As argued in Sec. II, the value of $S_{\text{entr}}^{\text{open}}$ is negligible in a first-order scheme (in Δt) such as this GMC model. However, note that the errors associated with neglecting S_{entr} will have minimum impact in regimes in which $\rho(S_{\text{proj}}^{\text{steady}})^{3/2} \sim M_{\text{tot}}$ (i.e., for personnel and cargo applications), given the fact that most of the peak inflation would have occurred well before $S(t)$ is reaching maximum area $S_{\text{proj}}^{\text{open}} + S_{\text{entr}}^{\text{open}}$ [2]. Thus, the errors on $S_{\text{entr}}^{\text{open}}$ should affect the calculated inflation time but not the maximum drag force.

Other necessary inputs are the following (namely, the so-called *at-the-loft* inputs):

Parafoil:

$$V(0), \quad M_{\text{tot}}, \quad \rho, \quad L_{\text{chord}}, \quad L(0) \text{ (initial span)}, \quad L_{\text{span}}$$

where L_{chord}, $L(0)$, and L_{span} are used to compute the initial and final collection reference area: namely, $S(0) \equiv L(0)L_{\text{chord}}$ and $S_{\text{final}} = L_{\text{span}}L_{\text{chord}}$.

Hemispherical canopy:

$$V(0), \quad M_{\text{tot}}, \quad \rho, \quad r(0), \quad D_0$$

In this case, the values of $S(0)$ and S_{final} are computed from $r(0)$ and R_{proj} via $S(0) = \pi r(0)^2$ and $S_{\text{final}} = (\pi/4)D_0^2$ (to allow for overinflation). Such at-the-loft parameters should, except for $V(0)$, be quite straightforward to measure. The values of $r(0)$ and $L(0)$ could be estimated by the riser separation distance, deployment bag width, or by any other length scales characterizing the dynamics that yield $S(0)$. On the other hand, the value of ρ shall be known from the knowledge of the drop altitude and of the prevalent meteorological conditions. As for $V(0)$, a separate computer simulation of the ballistic fall of a "draggy" rectangular box before inflation should yield an estimate accurate to about 10 to 20% (more on this point later).

In a typical numerical process, the quantity in curly brackets on the left-hand sides (LHSs) of Eqs. (12) and (13) will be known from the result of the previous iteration and will be used as an effective mass in the solution of a Newtonian equation of motion involving a force consisting of the V^2 term as the momentum-changing force. Most important, in both Eqs. (12) and (13), the actual duration of canopy expansion is calculated, not required as an input, because the numerical solution will be stopped via the tracking of $S(t)$, as discussed earlier.

The complete simulation of the trajectory of an inflating parachute does not stop at the end of inflation, but rather at the point of the canopy reaching steady-state descent. In the case of a strictly nongliding canopy, the transitory postinflation stage can be described by the following drag function evolution [21]:

$$C(t) = C^{\text{init}} \left| \frac{V(t)}{V_i} \right|^{\beta-2} \tag{14}$$

with

$$\beta = 2 + \frac{\ell_n\left(C^{\text{init}}/C_D^{\text{steady}}\right)}{\ell_n(V_i/V_T)} \tag{15}$$

The input parameters C_{init} and V_i are not user inputs, being obtained instead at the very last iteration step of the solution of Eq. (12) or Eq. (13) after $V(t)$ and $C(t)$ have been calculated [$C(t) \equiv 2F_D(t)/\rho S(t)V(t)^2$]. On the other hand, V_T and C_D^{steady} are the well-known descent rate and drag coefficient of the parachute payload during steady descent. Note that this postinflation model assumes that $C_{\text{init}} > C_D^{\text{steady}}$, a fact that may not always follow from Eqs. (12) and (13) in cases in which there is a lot of mass capture; a more detailed simulation, such as that of Spahr and Wolf [11], would be more appropriate in such cases. In the following comparison, it turns out that the use of Eqs. (14) and (15) is justified.

Note that Eq. (5) further justifies one assumption used in [21] to derive Eqs. (14) and (15): namely, that of $C(t)$ depending strongly on $V(t)$ and weakly on $a(t)$. During postinflation, mass capture is nearly total once again, with the captured mass ending up in the expanding near wake as a result of wake pileup. Because $S(t) = S$ (a constant) here, the integral in Eq. (5) is then calculated as

$$\int_0^t \mathrm{d}t' S(t')V(t') = S\int_0^t \mathrm{d}t' V(t') = SZ(t)$$

thus yielding $F_D = \rho S[V^2(t) + Z(t)a(t)]$: namely, a drag force depending on the velocity-dominated functions $V^2(t)$ and $Z(t)a(t)$.

Typical numerical solutions are presented in Figs. 3–9 using the canopy dimensions of the experimental systems discussed in the next

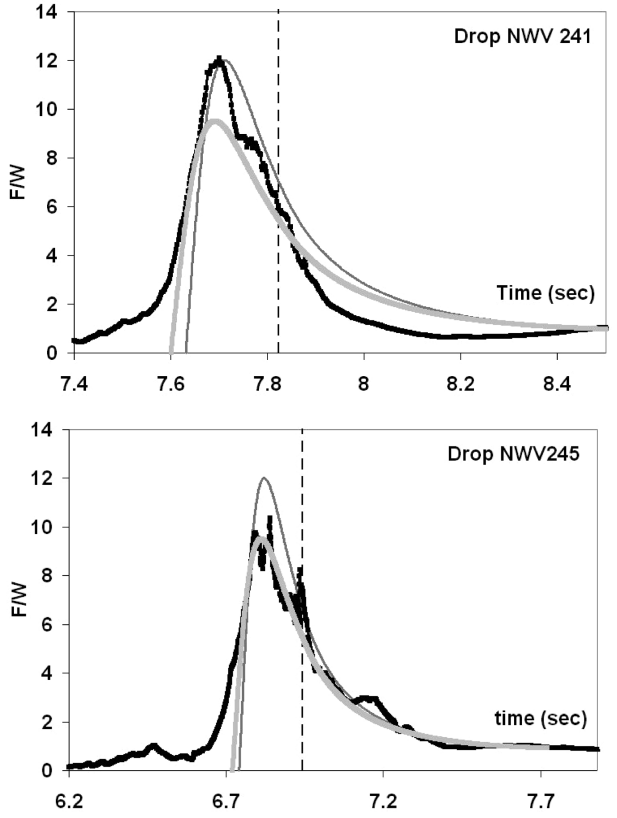

Fig. 3 Drag evolutions of the Strato Cloud parafoil, normalized to parachute payload weight. Experimental data are represented by the jagged curve, and the GMC simulations are represented by the two continuous curves [$V(0) = 124$ fps (high maximum) and 110 ft/s (lower maximum)]. The dashed line marks the end of the inflation phase. All other input parameters are listed in the text.

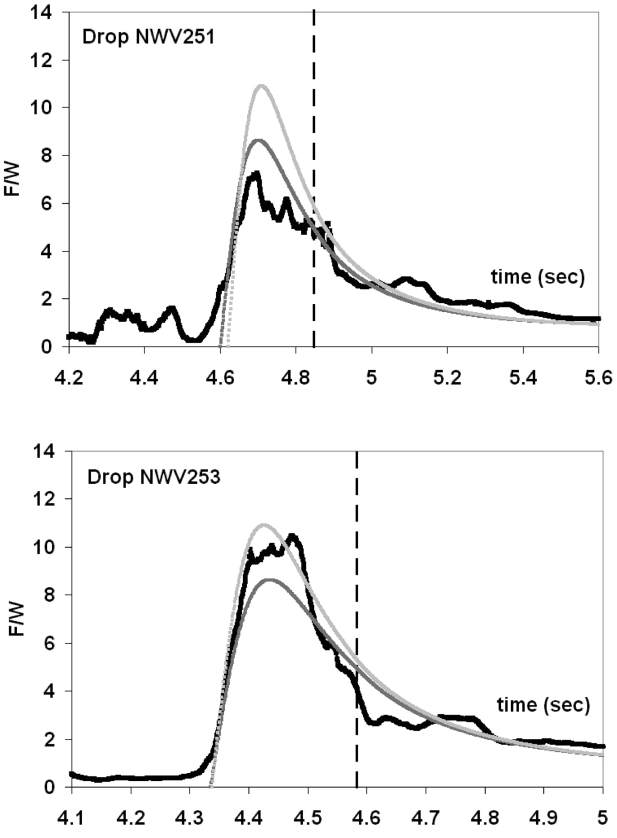

Fig. 4 Drag evolutions of the Falcon parafoil, normalized to parachute payload weight. The symbol convention follows that of Fig. 3.

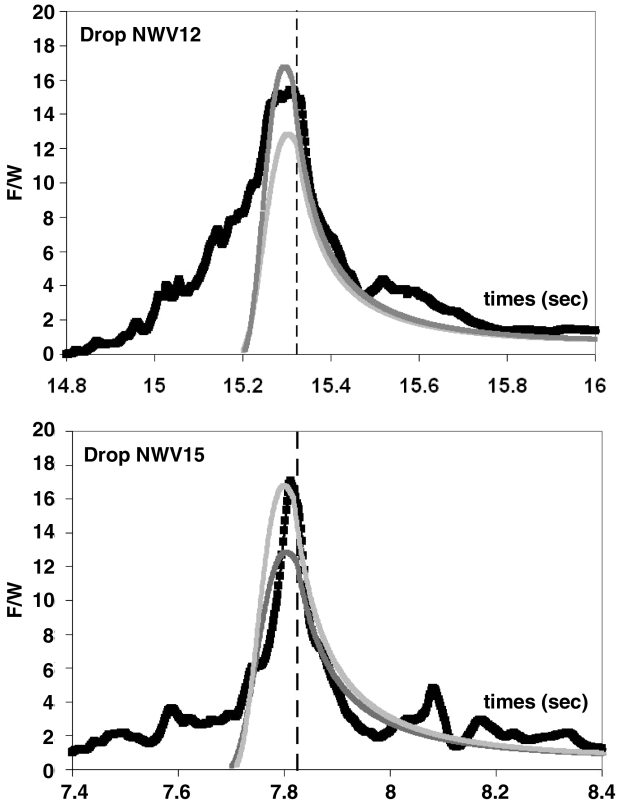

Fig. 5 Drag evolution of the half-scale C-9 hemispherical canopy, normalized to parachute payload weight. Experimental data are represented by the jagged curve, and the GMC simulations are represented by the two continuous curves [$V(0) = 119$ fps (high maximum) and 105 ft/s (lower maximum)]. The dashed line marks the end of the inflation phase. All other input parameters are listed in the text.

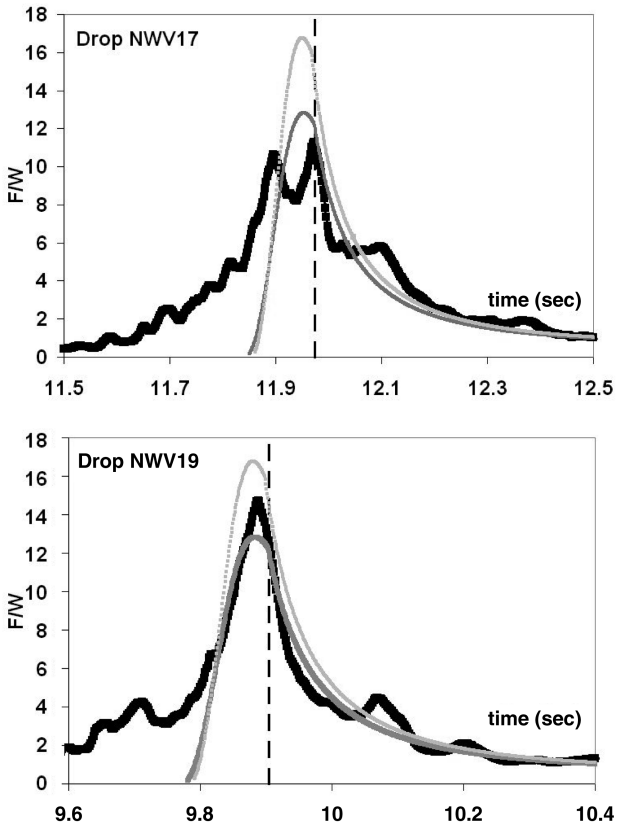

Fig. 6 Drag evolution of the half-scale C-9 hemispherical canopy, normalized to parachute payload weight. The symbol convention follows that of Fig. 5.

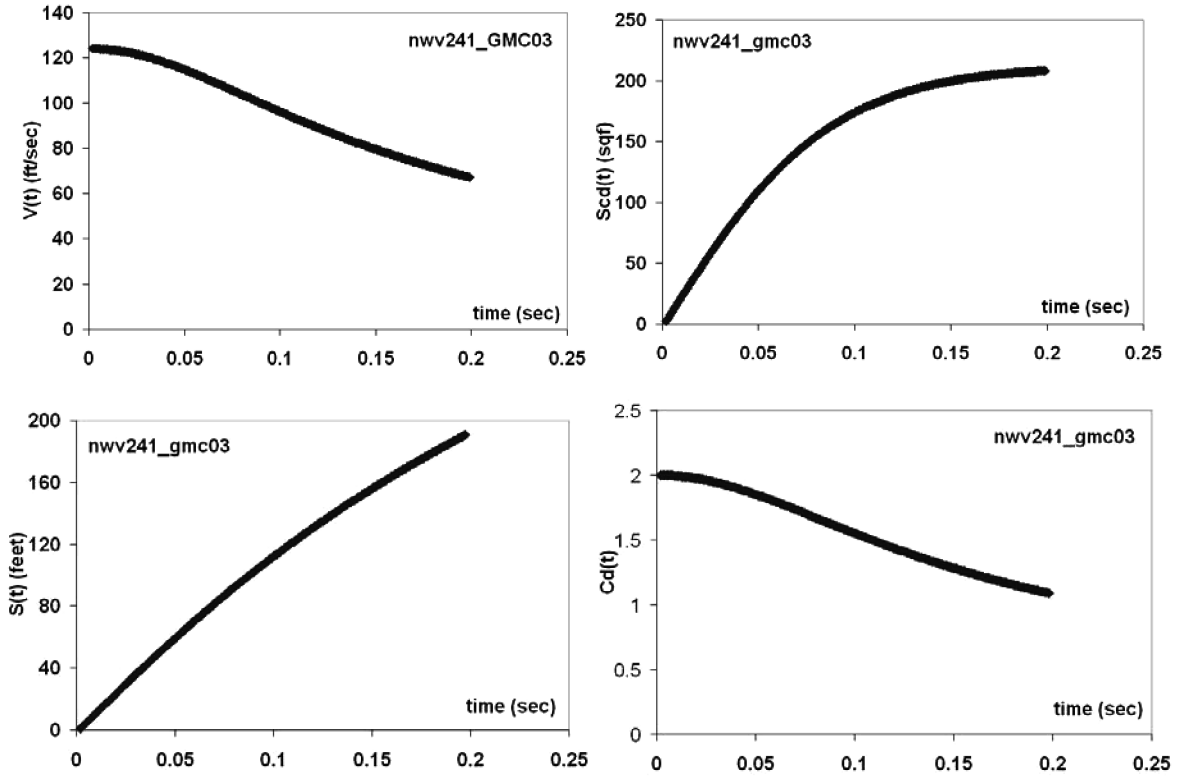

Fig. 7 GMC-based computations for the Strato Cloud parafoil.

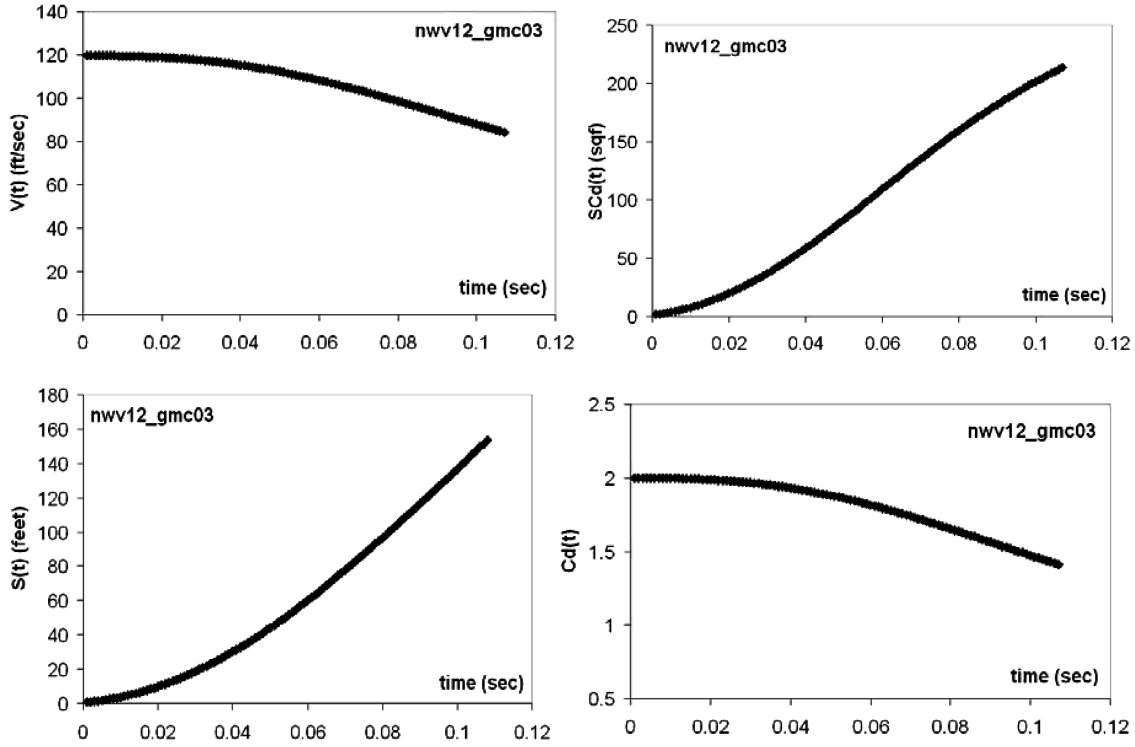

Fig. 8 GMC-based computations for the half-scale C-9 canopy.

section. These solutions were numerically obtained mostly from a simple Euler scheme performed at three values of the integration time step: namely, d$t = 0.001$, 0.005, and 0.01 s, which yielded solutions that differed only by very small amounts. Further checking was performed by comparing these solutions with those of another numerical solution of Eqs. (12) and (13), involving the commercial Mathcad spreadsheet program, which is based on a Runge–Kutta scheme. The results from the Euler scheme should be acceptable in this problem, given that the motion is not periodic and that it is controlled basically by only one timescale [i.e., $D_0/V(0)$], given the near-horizontal trajectories considered here. These simulations reveal the singly peaked shapes that are typical of inflating parachutes. Most interesting is the fact that the total inflation time, as well as the parachute's unsteady drag coefficient (see Figs. 7 and 8) are now calculated outputs rather than inputs.

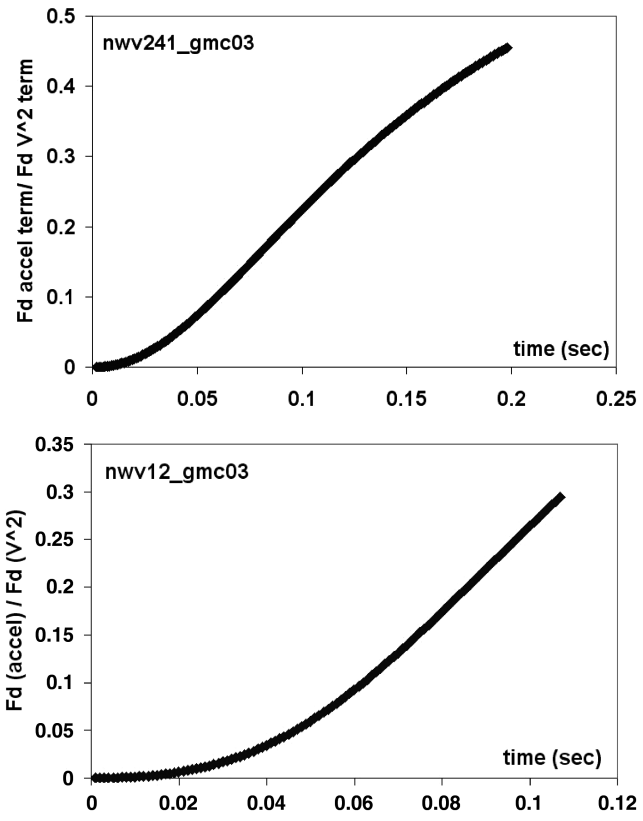

Fig. 9 Computed ratio of the added mass-to-form drag terms for the Strato Cloud parafoil (top) and the half-scale C-9 canopy (bottom).

IV. Comparisons with Experimental Data

The validity of the total mass capture idea, as well as of the various approximations used to produce a workable trajectory simulation, can be assessed directly with the comparison with the inflation data collected during the test drop programs reported by Potvin et al. [23,24]. These drops involved both canopy types, carrying total weights of 160 lb (parafoils) and 105 lb (hemispherical canopies). The ballast, together with the data gathering hardware, was located in steel tubs of dimensions $20.25 \times 32.00 \times 24.00$ in. The parachutes used in the study consisted of the following: a Para-Flite Strato Cloud parafoil canopy, used without its slider and built out of 7 cells sewn into a wing of 19.16-ft span and 10.08-ft chord, and a Precision Falcon 175 parafoil, again used without its slider, comprising 9 cells arranged into a wing of 21.25-ft span and 8.24-ft chord. More details concerning those two parafoils can be found in [3]. A third canopy used in the study was a half-scale version of a U.S. Air Force C-9 low-porosity hemispherical canopy, a 14-ft-diam flat circular design that was used previously in a study by Lee [25]. Note that swift and transverse inflation was insured for this C-9 model by connecting the canopy to a wider-than-usual payload as well as packing it in an oversized deployment bag (i.e., one for canopies that are twice as large).

All systems were dropped via a static line from the side door of Cessna aircraft (namely, models 402, 411, and 208), which were flying at 95–100 KIAS, and at about 800 ft over the ground of the Vandalia, Illinois, or Bowling Green, Missouri, municipal airports (about 500 ft above sea-level elevation in both cases). Parachute drag was measured by load cells attached to the risers, with errors estimated at about ± 10 lb. These force data were recorded by an

onboard data acquisition system at a rate of 1000 Hz. Each drop had video coverage to be used for the determination of the duration of parachute deployment as well as for an estimation of the parachute's (mouth) surface area at the beginning of the inflation process. This parachute drag data are also shown in Figs. 3–6. Interested readers may want to compare these curves with those of [4], which were collected on slowly (or nominally) opening canopies.

Note that the figures show repeat drops for each parachute (i.e., drop performed at the same suspended weight, same altitude and nearly the same aircraft speed, etc.). This is a crucial feature, given the drop-to-drop variations that are expected for the values of $V(0)$, $S(0)$, and, in principle, of Γ_{capt} as well.

A. Determination of the Initial Fall Rate and Canopy Dimensions

The values of $L(0)$ and $r(0)$ used in Figs. 3–6 were estimated from video at 0 ft (both parafoils) and 0.5 ft (half-scale C-9). The value of $V(0)$, on the other hand, could not be measured very accurately in the test setup used here. Instead, it was obtained from a numerical simulation of the fall, beginning after the payload box left the aircraft flying at a known speed, and including parachute deployment. Here, the box was modeled as generating both drag and lift. Figures 3–6 display two GMC solutions involving two different simulations of the preinflation fall, to yield values of $V(0)$ corresponding to the container generating (steady-state) drag only, and the container sustaining both steady-state drag and lift. In this last case, lift was modeled as arising from two flat plates joined at 90 deg with respect to each other (i.e., by the wind-facing faces of the box tilted at a small angle of attack). In both cases, the durations of the fall and deployment phases were known from video coverage (i.e., at about 0.5 s). Such preinflation simulations thus provided low- and high-end estimates of $V(0)$, a quantity that is, in fact, expected to be different on a drop-to-drop basis, depending on the tumbling dynamics of the box (a nonrepeatable process). The preinflation simulations yielded $V(0) = 110$ and 124 ft/s for both parafoils and $V(0) = 105$ and 119 ft/s for the half-scale C-9 canopy.

B. Hemispherical Canopy

Beginning with the case of the subscale C-9 hemispherical canopy, the comparisons shown in Figs. 5 and 6 suggest reasonable matches between the numerical and the experimental data for three of the four test drops that were carried out. The fact that the video of all four drops showed very similar evolutions of the canopy's shape points to a purely aerodynamic explanation for the drastic mismatch seen with drop NWV17, perhaps to significant shedding of the captured air before the end of inflation. This is not a far-fetched scenario given the stochastic character of the air captured in the near wake. Obviously, this scenario points to the fact that swift and transverse inflation may also operate under partial air mass capture.

The early stage of the inflation process, on the other hand, appears to be poorly reproduced in all cases. This could be reflected by the fact that the model does not include the drag generated by the sniveling (or flagging) canopy just before inflation. Such flagging drag could yield the low-force signal, as well as the rise early in the inflation process, seen before the moment of peak force. Moreover, neglecting S_{entr} early in the inflation process may yield a worse approximation, given that $S_{\text{proj}}(t)$ at that time could be small and of the same magnitude as $S_{\text{entr}}(t)$.

C. Parafoils

The data provided by the Strato Cloud and Falcon parafoils yield a somewhat different story: namely, that of satisfactory matches with only one canopy design (i.e., Strato Cloud). The fact that the GMC model does not work at all with the Falcon data suggests a possible systematic omission in the theory, possibly that of the wing's lift force not being included in Eq. (5) in the first place. Being built out of a 9-cell configuration and having a larger wing aspect ratio, the Falcon turns out to be a much better glider during steady descent than the 7-cell Strato Cloud. It is thus possible that the Falcon may still be in a gliding mode during inflation, unlike the Strato Cloud. Note that the steering lines of both canopies were rigged in a braking mode to minimize any propensity to glide, in this case rigged to the so-called half-brake setting. Brake setting is a rigging procedure by which the steering lines are constrained to a shorter length during inflation, yielding a deep cupping of the wing's trailing edge and a reduction of the evolving L/D. Such constraints are removed after inflation to allow maneuvering during the steady glide portion of the flight.[§]

Note finally that Figs. 3 and 4 include only those openings that were symmetrical (i.e., openings in which both right and left portions of the span extended at the same time). Several drops yielded asymmetrical openings with one side completely opening before the other, a process that produced strongly bipeaked drag evolution curves and lower maximum forces. Obviously, asymmetrical openings cannot be consistent with Eqs. (6–9), nor can they be expected to be well simulated by the mass capture idea discussed here.

D. Opening Shock Factor

The numerical data pertaining to the experimental data shown here can be used to obtain the value of the opening shock factor C_k previously discussed in Sec. II, yielding $C_k = 0.59$ for both Falcon and Stratostar parafoils and $C_k = 1.04$ for the half-scale C-9 canopy. Such values are about 300% lower than the predictions of Sec. II, which were made for much heavier payloads. These C_k values are also a bit higher than those discussed by Knacke [2], Ewing et al. [26], and Wolf [27] for canopies loaded in the same weight range as those discussed here. As explained in [4], higher values of C_k should, in fact, be expected for swift-opening canopies, given that C_k is inversely proportional to inflation time and that the parachutes of Figs. 3–6 inflate at much higher rates than those of [2,26,27].

E. GMC Assessment

The matches of Figs. 3, 5, and 6 do show how well the GMC model can reproduce the general height and width of the drag-vs-time curve near the time of peak drag, as well as the drag letdown after peak drag. Note that this feat was achieved *without* the tuning of any of the input parameters, including $V(0)$ and Γ_{capt}, as would have been done in a curve-fitting approach. This contrasts with models that use explicit added mass terms of the type $M_{\text{air}}\,\mathrm{d}V/\mathrm{d}t$ and $V\,\mathrm{d}M_{\text{air}}/\mathrm{d}t$ [7–17], which do require the tuning of the coefficient(s) related to the explicit forms used for M_{air}. This is a problematic proposition because these coefficients are intrinsically of a dynamic nature (i.e., depending on the specifics of the flow into and around the parachute). On the other hand, the fact that the GMC model missed the cases represented by the Falcon parafoil, as well as those of drop NWV17, does point to the inflation process, however swift, not being always being described by total mass capture. This, of course, is not surprising, given the complex nature of parachute inflation in general.

F. Linear Versus Quadratic Inflation

Interesting comparisons between the mass capture dynamics of parafoils and of hemispherical canopies are shown in Figs. 7–9, as obtained from the numerical simulations of the Strato Star parafoil and half-scale C-9 canopy. In both cases, the higher simulated value of $V(0)$ was used: namely, 124 and 119 ft/s, respectively. Of interest in both figures are the evolutions, *during inflation*, of the drag area $SC_D(t) \equiv 2F_D(t)/\rho V^2(t)$, of the instant drag coefficient $C_D(t) \equiv SC_D(t)/S(t)$ [with $S(t)$ computed from Eqs. (10) and (11)], and of the ratio R_{Fd} of the added mass term (i.e., the terms in $\mathrm{d}V/\mathrm{d}t$), to the form drag term (i.e., term in V^2) appearing in Eq. (5). This last ratio would be given, in the case of parafoils, by

[§]Note that the cupping of the wing's trailing edge corresponding to a half-brake setting is less pronounced without slider reefing than with it. This is because with sliders, the steering lines are routed through the sliders' back side; because slider chord is usually much smaller than the wing's chord, the constrained steering lines thus pull-in further the trailing edge of the entire canopy.

$$R_{\mathrm{Fd}} \equiv -1\left\{\Gamma_{\mathrm{capt}}\rho\left(\frac{Z(t)^2 L_{\mathrm{chord}}}{2n_p} + S(0)Z(t)\right)\left(\frac{\mathrm{d}^2 Z}{\mathrm{d}t^2}\right)\right\} \Bigg/ \left\{2\left(\frac{Z(t)L_{\mathrm{chord}}}{n_p} + S(0)\right)\frac{\rho V^2}{2}\right\}$$

Overall, comparing Figs. 6 and 7 shows somewhat different concavities for all quantities plotted. This result is partly the reflection of parafoils expanding linearly (i.e., in one direction only) and of hemispherical canopies opening in a quadratic manner (i.e., over two directions).

Most noticeable are the opposite concavities of $S(t)C_D(t)$, $S(t)$, and $C_D(t)$. The comparison of the drag term ratio R_{Fd} in Fig. 9 is also interesting, but perhaps only superficially. Indeed, noticing that R_{Fd} is basically the ratio of a factor proportional to volume over a factor proportional to surface area, one expects this ratio to scale, at the end of inflation, to a value that is proportional to overall size. Given the actual values of both parafoil spans (i.e., ~20 ft) and the nominal diameter of the half-scale C-9 (i.e., 14 ft), such endpoint values should thus compare in a proportion equal to 20 ft/14 ft ~ 1.4, which appears to be the case, judging from the endpoint values shown in the figure, for which $R_{\mathrm{Fd}}^{\mathrm{strato}}/R_{\mathrm{Fd}}^{\mathrm{c\text{-}9}} \sim 0.47/0.31 \sim 1.5$. This example shows that canopy size is also a major contributor to the added mass term, perhaps as important as canopy shape and porosity.

This discussion also shows that the contrasts in the evolutions of the collection area $S(t)$ and of the drag function $C_D(t)$ between the two canopy types are rather subtle and are due to several factors *in addition to* basic canopy geometry differences. This can be seen more clearly by looking at the opening shock factor, as discussed next.

V. Nondimensional Formulation and Mass-Ratio Scaling Study

The evaluation of the degree of realism of any inflation model over wide ranges of input parameter values can always be assessed efficiently and economically when considering nondimensional formulations of both model and input parameters. For inflation studies, such a formulation can be guided by the opening shock factor $C_k (\equiv F_D^{\max}/(C_{D0}S_0 q(0)))$ discussed in Sec. II, given the large database that is associated with it already [2,26,27]. As discussed in [4], the values of C_k collapse onto distinct narrow bands when plotted, at fixed nondimensional inflation time, with respect to the so-called inverse mass ratio $R_m^{(\mathrm{adj})} (\equiv \rho(C_{D0}S_0)^{3/2}/M_{\mathrm{tot}})$. Arising from the well-known impulse-momentum theorem, such scaling behavior should be quite general and reflected in the GMC model as well, given that the latter has no usage restrictions with regard to mass ratio (being based on specific fluid flows instead). Formulating the GMC model in a nondimensional manner to reflect mass-ratio dependence is hereby done as follows.

Using the generic length scale D and the system's initial fall rate $V(0)$ to define dimensionless distance and timescales, Eqs. (12) and (13) become

Parafoil:

$$D \equiv \sqrt{S_{\mathrm{open}}} \qquad Z \equiv D\tilde{Z} \qquad t \equiv \frac{D}{V(0)}\tilde{t}$$
$$R_m^{(p)} \equiv \frac{\rho L_{\mathrm{chord}} D^2}{M_{\mathrm{tot}}} \qquad R_{\mathrm{para}} \equiv n_p \frac{S(0)}{DL_{\mathrm{chord}}} \tag{16}$$
$$\tilde{A}_{\mathrm{ext}} \equiv \frac{F_{\mathrm{ext}}}{M_{\mathrm{tot}}}\frac{D}{V(0)^2}$$

$$\frac{\mathrm{d}^2\tilde{Z}}{\mathrm{d}\tilde{t}^2} = -\left(\frac{1}{n_p}\right)R_m^{(p)}[\tilde{Z} + R_{\mathrm{para}}]\left(\frac{\mathrm{d}\tilde{Z}}{\mathrm{d}\tilde{t}}\right)^2 - \left(\frac{\Gamma_{\mathrm{capt}}}{2n_p}\right)R_m^{(p)}[\tilde{Z} + 2R_{\mathrm{para}}]\tilde{Z}\frac{\mathrm{d}^2\tilde{Z}}{\mathrm{d}\tilde{t}^2} + \tilde{A}_{\mathrm{ext}} \tag{17}$$

Hemispherical canopy:

$$R_m^{(h)} \equiv \frac{\rho D^3}{M_{\mathrm{tot}}} \qquad R_{\mathrm{hemi}} \equiv n_h^2 \frac{S(0)}{D^2} \tag{18}$$

$$\frac{\mathrm{d}^2\tilde{Z}}{\mathrm{d}\tilde{t}^2} = -\left(\frac{1}{n_h^2}\right)R_m^{(h)}[\tilde{Z}^2 + 2\sqrt{R_{\mathrm{hemi}}}\tilde{Z} + R_{\mathrm{hemi}}]\left(\frac{\mathrm{d}\tilde{Z}}{\mathrm{d}\tilde{t}}\right)^2 - \left(\frac{\Gamma_{\mathrm{capt}}}{3n_h^2}\right)R_m^{(h)}[\tilde{Z}^2 + 3\sqrt{R_{\mathrm{hemi}}}\tilde{Z} + 3R_{\mathrm{hemi}}]\tilde{Z}\frac{\mathrm{d}^2\tilde{Z}}{\mathrm{d}\tilde{t}^2} + \tilde{A}_{\mathrm{ext}} \tag{19}$$

Here, the definitions for $\tilde{z}$, $\tilde{t}$, and $\tilde{A}_{\mathrm{ext}}$ in Eq. (19) are the same as in Eq. (17). Note that the mass ratio $R_m^{(\mathrm{adj})}$ has been replaced with $R_m^{(p)}$ and $R_m^{(h)}$, which are more natural to GMC. This is so given that the very concept of steady-state drag used in $R_m^{(\mathrm{adj})}$ never appears in the GMC approach. Note also that the LHSs of Eqs. (17) and (19) correspond to the dimensional product $M_{\mathrm{tot}}\,\mathrm{d}V/\mathrm{d}t$, and the first two terms of the RHSs correspond to the drag force $F_D(t)$. Given that Γ_{capt} and n_p are fixed (i.e., equal to 1), the specific evolution resulting from Eqs. (17) and (19) shall, in general, be determined by the values of the mass ratio $R_m^{(p)}$ (or $R_m^{(h)}$), the initial surface area ratio R_{para} (or R_{hemi}), and the acceleration modulus $\tilde{A}_{\mathrm{ext}}$. For example, the larger the mass ratio and/or the surface area ratio, the greater the influence of the drag force in decelerating the motion of the parachute payload system. On the other hand, the larger the external force F_{ext}, the less effective drag becomes as an agent of deceleration. Note also that large values of R_{para} (or R_{hemi}) will result in shorter inflation times, given that a larger $S(0)$ means higher fluxes at the canopy mouth.

Equations (17) and (19) yield interesting insight in cases when $F_{\mathrm{ext}} \sim 0$, for example, with canopies inflating mostly along the horizontal. In particular, the one interesting result follows when the initial opened surface area of the canopy is very small: that is, when $R_{\mathrm{para}} \sim R_{\mathrm{hemi}} \sim 0$ (actually, quite a realistic limit). In this case, the dynamics of Eqs. (17) and (19) are completely specified by the mass ratios $R_m^{(p)}$ and $R_m^{(h)}$, as shown explicitly here.

Parafoil:

$$\frac{\mathrm{d}^2\tilde{Z}}{\mathrm{d}\tilde{t}^2} \approx -\left(\frac{1}{n_p}R_m^{(p)}\right)\tilde{Z}\left[\left(\frac{\mathrm{d}\tilde{Z}}{\mathrm{d}\tilde{t}}\right)^2 + \Gamma_{\mathrm{capt}}\left(\frac{1}{2}\right)\tilde{Z}\frac{\mathrm{d}^2\tilde{Z}}{\mathrm{d}\tilde{t}^2}\right] \tag{20}$$

Hemispherical canopy:

$$\frac{\mathrm{d}^2\tilde{Z}}{\mathrm{d}\tilde{t}^2} = -\left(\frac{1}{n_h^2}R_m^{(h)}\right)\tilde{Z}^2\left[\left(\frac{\mathrm{d}\tilde{Z}}{\mathrm{d}\tilde{t}}\right)^2 + \Gamma_{\mathrm{capt}}\left(\frac{1}{3}\right)\tilde{Z}\frac{\mathrm{d}^2\tilde{Z}}{\mathrm{d}\tilde{t}^2}\right] \tag{21}$$

Given that $F_{\mathrm{ext}} = 0$, the entire RHSs of Eqs. (20) and (21) correspond to the nondimensional drag force $\tilde{F}_D$, defined here via $F_D(t) \equiv \tilde{F}_D(\tilde{t})M_{\mathrm{tot}}V(0)^2/D$. From this definition, the opening shock factor follows as $C_k = (2\tilde{F}_D^{\max}/R_m^{(\mathrm{adj})}) \cdot \sqrt{C_d^{\mathrm{steady}}}$. Given that Eqs. (20) and (21) depend on $R_m^{(p,h)}$ only (because, again, $\Gamma_{\mathrm{capt}} = 1$), one expects C_k to be indeed a function of mass ratio (and on C_D^{steady}) only, although not always in a manner proportional to $R_m^{(p,h)}$, because $\tilde{Z}$ is also dependent on $R_m^{(p,h)}$.

The specific dependence of C_k on $R_m^{(\mathrm{adj})}$ can be calculated over a wide range of mass ratios, via several computer simulations of either Eqs. (20) and (21) or Eqs. (12) and (13) (with $F_{\mathrm{ext}} = 0$), resulting in the data shown in Fig. 10. Here, $R_m^{(\mathrm{adj})}$ is used instead of $R_m^{(p,h)}$ to allow a direct comparison with [2,26,27]. Such simulations were carried out first using all input data but the mass M_{tot} for the half-scale C-9 and Strato Cloud canopies discussed in the previous section. Here, the mass ratio was changed by using different payload weights for each simulation (from 105 to 250,000 lb, the latter to simulate the zero-mass-ratio condition). Moreover, two initial collection reference areas $S(0)$ of 0.79 ft^2 and 28 ft^2 were used for the case of the half-scale C-9 to indicate the extent of the variation of C_k with respect to initial opened collection areas. Note that initial speeds other than those of Sec. III were used as well, to further widen the database, by performing simulations with $V(0)$ in the range of 100–250 ft/s. Such speeds were chosen to remain in the range of inflation times of order $\sim D/V(0)$, as demanded by the GMC

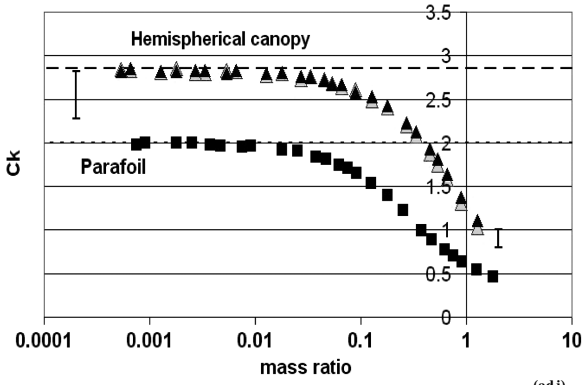

Fig. 10 Calculated opening shock factor versus mass ratio $R_m^{(adj)}$. The dash-dot and dashed lines represent the zero-R_m limits predicted in Sec. II. The triangles correspond to $r(0) = 0.5$ and 3.0 ft, respectively. The rest of the simulation inputs are discussed in the text. The error bars correspond to the uncertainty related to the overinflation area for hemispherical canopies.

approach, and to also stay within the accuracy constraints of the numerical techniques used to solve the equations of motion. Finally, note that the scaling curves of Fig. 10 have incorporated the two zero-R_m limits discussed in Sec. II. The error bars shown here correspond to the 20% uncertainty associated with the determination of the overinflation ratio $S_{\text{proj}}^{\text{open}}/S_0$ in the case of hemispherical canopies (the two error bars shown correspond to the $R_m^{(adj)} \sim 0$ and ~ 1 cases, respectively).

Returning to the issue of linear versus quadratic inflation, the superposition of the scaling curves for both parafoil and hemispherical canopies now show a marked distinction between the two designs. Most important, the comparison is made for the two canopy types inflating at the same timescale [i.e., $D/V(0)$], a fact that allows the conclusion that, indeed, hemispherical canopies do generate a larger peak inflation drag (relative to their steady-state drag) than parafoils.

Comparing the numerical data of Fig. 10 with that of the latest compilation by Wolf [27] of C_k values of fast-disreefing inflating parachutes (also reproduced in [4]), the following trends are observed:

1) There is a similar increase and then the saturation of C_k at decreasing mass ratios, starting with similar values at mass ratios near unity. Note that the data scatter is similar in both cases as well, reflecting the fact that different canopy designs are being compared in both studies (Wolf [27] is comparing canopies of different porosities). Note also that Wolf's database, being of an experimental nature, incorporates additional scatter arising from the anticipated drop-to-drop variations in the actual amount of air being captured.

2) There are strikingly different zero-mass-ratio limits, with plateaus located in the 2.0–2.8 range with the GMC approach, versus plateaus in the 1.0–1.5 range in Wolf's [27] compilation. This is understood again from the fact that C_k is quite sensitive on opening time and the fact that the canopies modeled by GMC open at rates that are much faster than even the fast openers studied in [27].

Finally, the results of Fig. 10 can also be compared with Wolf's [27] opening shock factor compilation of unreefed parachute openings (all low- and high-porosity hemispherical canopies), which are 5 to 10 times slower than swift openings [27]. Here, the difference is even more striking, beginning at $R_m^{(adj)} \sim 1$, where $C_k \sim 0.1$, and ending at the $C_k \sim 1.0$–1.5 level as $R_m^{(adj)} \to 0$. But, again, the difference has more to do with the inflation timescales being very different, rather than the realism value of the GMC approach. On the other hand, the comparison shows quite clearly that C_k is mainly driven by mass ratio and opening times.

VI. Conclusions

This paper has shown that using the idea of total and instant mass capture yields a useful tool for the investigation of rare but potentially destructive modes of parachute inflation. In particular, the GMC model makes several predictions concerning the value of the opening shock factor C_k over a wide range of mass ratios (Fig. 10), predictions that should be straightforward to confirm or refute by wind-tunnel experiments and test drops. Although restricted to a specific inflation mode, the model also provides the first-ever derivation from basic aerodynamic principles of several fundamental characteristics of the parachute drag during opening: namely, 1) its dependence in terms of the inverse mass ratio [Eqs. (17–21)], 2) the evolution of the drag coefficient over time (Figs. 7 and 8), and 3) the fundamental differences between canopies that inflate radially and those that inflate linearly.

On the other hand, a comparison with experimental data has shown that total mass capture may indeed occur with swiftly inflating canopies, although not on every drop, even when repeated under the same conditions. This suggests the sporadic, rather than recurrent, character of total mass capture even during swift inflation. This conclusion may diminish the appeal of the GMC model as a predictive tool for swift inflation. But given that partial mass capture typically yields lower inflation forces compared with total capture, the GMC model is truly a tool for the investigation of worse-case scenarios.

Further study of the GMC-related ideas and approximations is needed, of course. Foremost should be the issue of transverse and swift inflation being a sufficient criterion for complete mass capture. As seen with the Falcon experimental data, residual lift may generate transverse (i.e., back and forth) motions that actually prevent complete mass capture by moving the canopy away from entrained air. On the other hand, whether mass capture is achieved (for strictly nongliding canopies) whenever $t_{\text{infl}} \sim D/V(0)$ should be checked as well [i.e., for a wide range of $V(0)$, including very low values of $V(0)$]. Finally, the neglecting of the momentum transfer in/out of the potential-flow streamlines should be further assessed. This could be achieved by using the force and flow measurements collected during a detailed wind-tunnel study of a swiftly opening parachute model, along the lines described in [18], in concert with a numerical solution of the inviscid fluid equations of the flow around the canopy *and* wake, as proposed recently by Johari and Desabrais [28].

Specific improvements of the GMC model should also be contemplated. These should include a physically based model of the evolution of the entrainment area S_{entr}, to at least get the early inflation stage right, and a physically based picture of the relation between the evolution of the collection area $S(t)$ and the parachute payload travel distance $Z(t)$. The latter is needed to replace Eqs. (6) and (7), which although qualitatively true, probably miss interesting canopy expansion dynamics. In the case of parafoils, for example, such a model could track the transverse motion of the wing tips, as controlled by the balance between the high pressure residing under the bottom skin of the canopy and the impact force of the air that is hitting the stabilizers from the outside.

Acknowledgments

This work was performed with funding from the U.S. Army Natick Soldier Center (Natick, MA) under U.S. Army contract W9124R-07-P-1156. The author wishes to thank the following individuals with whom he has enjoyed many fruitful discussions: G. Peek from Industrologic, Inc., R. Charles and K. Desabrais from the U.S. Army Natick Soldier Center, and H. Johari from California State University, Northridge.

References

[1] Potvin, J., Peek, G., and Brocato, B., "Modeling the Inflation of Ram-Air Parachutes Reefed with Sliders," *Journal of Aircraft*, Vol. 38, No. 5, 2001, pp. 818–827.

[2] Knacke, T. W., *Parachute Recovery Systems Design Manual*, Para Publishing, Santa Barbara, CA, 1992.

[3] Poynter, D., *The Parachute Manual*, 4th ed., Vols. 1–2, Para Publishing, Santa Barbara, CA, 1991.

[4] Potvin, J., "Universality Considerations for Graphing Parachute Opening Shock Factor Versus Mass Ratio," *Journal of Aircraft*, Vol. 44, No. 2, 2007, pp. 528–538.

doi:10.2514/1.24061
[5] Potvin, J., "Momentum-Impulse Balance and Parachute Inflation: Dis-Reefing," *Journal of Aircraft*, Vol. 44, No. 2, 2007, pp. 691–694. doi:10.2514/1.26286
[6] Lamb, H., "On the Motion of Solids Through a Liquid," *Hydrodynamics*, 6th ed., Dover, New York, 1945, pp. 160–201.
[7] Sarpkaya, T., "Method of Analysis for Flow Around Parachute Canopies," 11th AIAA Aerodynamic Decelerator Systems Technology Conference, AIAA, Reston, VA, AIAA Paper 91-0825, 1991, pp. 1–17.
[8] Wolf, D. E., "A Simplified Dynamic Model of Parachute Inflation," *Journal of Aircraft*, Vol. 11, Jan. 1974, pp. 28–33. doi:10.2514/3.60317
[9] McVey, D. F., and Wolf, D. E., "Analysis of Deployment and Inflation of Large Ribbon Parachutes," *Journal of Aircraft*, Vol. 11, Feb. 1974, pp. 96–103. doi:10.2514/3.60329
[10] Macha, J. M., "A Simple Approximate Model of Parachute Inflation," 12th RaeS/AIAA Aerodynamic Decelerator Systems Technology Conference and Seminar, London, AIAA Paper 93-1206, May 1993.
[11] Spahr, H. R., and Wolf, D. F., "Theoretical Analysis of Wake-Induced Parachute Collapse," 7th AIAA Aerodynamic Decelerator and Balloon Technology, San Diego, CA, AIAA Paper 81-1922, Oct. 1981.
[12] Lingard, J. S., "The Effects of Added Mass on Parachute Inflation Force Coefficients," *13th AIAA Aerodynamic Decelerator Systems Technology Conference*, AIAA, Washington, D.C., 1995, pp. 176–185; also AIAA Paper 95-1561, 1995.
[13] O'Hara, F., "Notes on the Opening Behavior and the Opening Forces of Parachutes," *Journal of the Royal Aeronautical Society*, Vol. 53, Nov. 1949, pp. 1053–1062.
[14] Heinrich, H. G., and Noreen, R. A., "Analysis of Parachute Dynamics with Supporting Wind Tunnel Experiments," 7th AIAA Aerodynamic Decelerator and Balloon Technology Conference, El Centro, CA, AIAA Paper 68-924, 1968.
[15] Heinrich, H. G., "Opening Time of Parachutes Under Infinite-Mass Conditions," *Journal of Aircraft*, Vol. 6, May–June 1969, pp. 268–272. doi:10.2514/3.44047
[16] Payne, P. R., "A New Look at Parachute Opening Dynamics," *The Aeronautical Journal*, Vol. 75, Feb. 1973, pp. 85–93.
[17] Maydew, R. C., and Petwerson, C. W., *Design and Testing of High-Performance Parachutes*, edited by K. J. Orlik-Ruckermann, AGARD, AGARDograph 319, Neuilly-sur-Seine, France, Nov. 1991.
[18] Desabrais, K. J., and Johari, H., "Unsteady Potential Flow Forces on an Inflating Parachute Canopy," 17th AIAA Aerodynamic Decelerator Systems Technology Conference, Monterey, CA, AIAA Paper 2003-2144, 19–22 May 2003.
[19] Desabrais, K. J., Johari, H., and Lee, C. K., "Effects of Inflation Dynamics on the Drag of Round Parachute Canopies," 19th AIAA Aerodynamic Decelerator Systems Technology Conference, Monterey, CA, AIAA Paper 2007-2562, 21–24 May 2007.
[20] Potvin, J., Papke, J., Brighton, E., Farmer, M., and Peek, G., "A New Inflation Model for Low-Porosity Hemispherical Parachutes: Validation and Implementation in PIMS V3.0," 18th AIAA Aerodynamic Decelerator Systems Conference and Seminar, Munich, Germany, AIAA Paper 2005-1687, May 2005.
[21] Potvin, J., Peek, G., and Brocato, B., "New Model of Decelerating Bluff Body Drag," *Journal of Aircraft*, Vol. 40, No. 2, 2003, pp. 370–377.
[22] Potvin, J., "Momentum-Impulse Balance and Parachute Inflation: Rocket-Propelled Payloads," *Journal of Aircraft*, Vol. 44, No. 3, 2007, pp. 1039–1042. doi:10.2514/1.27481
[23] Potvin, J., and Peek, G., "Inflation Study of U.S. Army Parachutes," U.S. Army CR W9124R-04-P-1272, Yuma Proving Ground, Yuma, AZ, 21 Apr. 2005.
[24] Potvin, J., Peek, G., Brocato, B., Kutz, R., Manglano, C., and Yavitz, B., "Deceleration Dynamics of Unreefed Cruciform and Flat Circular Parachutes During and After Inflation," 16th AIAA Aerodynamic Decelerator Systems Technology Conference and Seminar, Boston, MA, AIAA Paper 2001-2028, May 21–24 2001, pp. 224–234.
[25] Lee, C. K., "Experimental Investigation of Full-Scale and Model Parachute Opening," 8th AIAA Aerodynamic Decelerator and Balloon Technology Conference, Hyannis, MA, AIAA Paper 84-0820, Apr. 2–4, 1984.
[26] Ewing, E. G., Bixby, H. W., and Knacke, T. W., "Recovery Systems Design Guide," U.S. Air Force Flight Dynamics Lab., Rept. AFFDL-TR-78-151, Wright–Patterson AFB, OH, Dec. 1978 pp. 254–257.
[27] Wolf, D., "Opening Shock," 15th CEAS/AIAA Aerodynamic Decelerator Systems Technology Conference, Toulouse, France, AIAA Paper 99-1702, 8–11 June 1999.
[28] Johari, H., and Desabrais, K. J., "A Coupled Fluid-Structure Parachute Inflation Model," 17th AIAA Aerodynamic Decelerator Systems Technology Conference, Monterey, CA, AIAA Paper 2003-2146, 19–22 May 2003.